# Compound and quasicompound states in low-energy scattering of nucleons from $^{12}$C

G. Pisent,[1,*] J. P. Svenne,[2,†] L. Canton,[1,‡] K. Amos,[3,§] S. Karataglidis,[3,¶] and D. van der Knijff[4,**]
[1]*Dipartimento di Fisica dell'Università di Padova and Istituto Nazionale di Fisica Nucleare, Sezione di Padova, via Marzolo 8, Padova I-35131, Italia*
[2]*Department of Physics and Astronomy, University of Manitoba, and Winnipeg Institute for Theoretical Physics, Winnipeg, Manitoba, Canada R3T 2N2*
[3]*School of Physics, University of Melbourne, Victoria 3010, Australia*
[4]*Advanced Research Computing, Information Division, University of Melbourne, Victoria 3010, Australia*
(Received 31 January 2005; published 5 July 2005)

A multichannel algebraic scattering theory has been used to study the properties of nucleon scattering from $^{12}$C and of the subthreshold compound nuclear states. The theory accounts for properties in the compound nuclei to ∼10 MeV. All compound and quasicompound resonances observed in total cross-section data are matched, and, on seeking solutions of the method at negative energies, all subthreshold states in $^{13}$C and $^{13}$N are predicted with the correct spin-parities and with reasonable values for their energies. A collective-model prescription has been used to define the initiating nucleon-$^{12}$C interactions and, via use of orthogonalizing pseudopotentials, account is made of the Pauli principle. Information is extracted on the underlying structure of each state in the compound systems by investigating the zero-deformation limit of the results.

DOI: 10.1103/PhysRevC.72.014601 PACS number(s): 24.10.−i, 25.40.Dn, 25.40.Ny, 28.20.Cz

## I. INTRODUCTION

In a recent paper [1], a multichannel algebraic scattering (MCAS) theory for nucleons scattering from a nucleus was specified in detail. At low energies, the approach is noteworthy because its formulation facilitates a systematic determination both of the subthreshold bound states and of the compound resonances. The theory is built upon Sturmian expansions of whatever one chooses to be an interaction matrix of potential functions [2]. Of course, there is the usual limitation of coupled channel problems, namely, that the dimension of the evaluation rapidly increases with the number of channels considered. However, the MCAS approach does treat all selected channels equivalently, whether they be open or closed, so that solutions can be found at both positive (scattering) and negative (bound system) energies relative to the nucleon on nucleus threshold.

Whereas the MCAS approach may be used for any target (and projectile) system, our formulation to date has been for nucleon-nucleus interactions. However, the most practical adaptations insofar as size of the problem and, concomitantly, computation times, are with light mass targets. They have well-separated low excitation spectra and usually the total cross-section data show distinct resonances upon a smooth background. Thus the first MCAS study [1] was of low-energy neutron-$^{12}$C ($n + {}^{12}$C) scattering. For that only three states of $^{12}$C ostensibly were needed in the evaluations: the $0^+_1$ (ground), the $2^+_1$ (4.4389 MeV), and the $0^+_2$ (7.6542 MeV). Herein we consider that same system in more detail and, as well, analyze proton-$^{12}$C ($p + {}^{12}$C) data.

The MCAS method solves the coupled-channel Lippmann-Schwinger equations for the nucleon-nucleus system considered. The starting matrix of potentials may be constructed from any nuclear model: shell or collective, rotational or vibrational. We have used a rotational collective-model representation for the interaction potential matrix but therein take deformation to second order. We have chosen Woods-Saxon functions and their various derivatives to be the form factors for all components each with characteristic operators of central, spin-orbit ($\mathbf{l}\cdot\mathbf{s}$), orbit-orbit ($\mathbf{l}\cdot\mathbf{l}$), and spin-spin ($\mathbf{s}\cdot\mathbf{I}$) type. The interactions were allowed to depend on parity as well. With such a characterization, the model potential is sufficiently flexible to describe all possible structures (at both positive and negative energies) of the nucleon-$^{12}$C system. However, any such collective-model prescription violates the Pauli principle. At these energies that violation is severe. But it is possible [1,3] in the MCAS approach to account for Pauli blocking of occupied nucleon states in the target, with this or any collective-model specification of the matrix of potentials. That is achieved by introducing orthogonalizing pseudopotentials [3–5] (OPP) into the scheme by which the Sturmians are specified. In that way all Sturmians in the (finite) set selected as the basis of expansion of the matrix of potentials contain few or no components equivalent to the external nucleon being placed in an already densely occupied orbit. Treatment of the Pauli principle has a significant effect on results [1,3].

The aim of this paper is to extend calculations from the $^{13}$C to the $^{13}$N system and to carry out a comparative analysis of the bound and resonance spectra involved. A second version of the program has been set up that can deal on the same footing with the scattering of neutrons and protons from the target nucleus. The neutron results confirm those of Ref. [1].

*Electronic address: gualtiero.pisent@pd.infn.it
†Electronic address: svenne@physics.umanitoba.ca
‡Electronic address: luciano.canton@pd.infn.it
§Electronic address: amos@physics.unimelb.edu.au
¶Electronic address: kara@physics.unimelb.edu.au
**Electronic address: dirk@unimelb.edu.au

 

TABLE I. $n + {}^{12}$C potential parameters (strengths in MeV).

| Parity | Central | Orbit-orbit | Spin-orbit | Spin-spin |
|---|---|---|---|---|
| − | −49.1437 | 4.5588 | 7.3836 | −4.7700 |
| + | −47.5627 | 0.6098 | 9.1760 | −0.0520 |
| Other parameters | $r_0 = 1.35$ fm | $a_0 = 0.65$ fm | $\beta_2 = -0.52$ | |

It will be shown that, in the $n + {}^{12}$C process, the spectrum of resonances up to about 6 MeV [in the laboratory (lab) system] is almost completely described by a mechanism involving excitation of the first $2^+$ level of $^{12}$C with energy $\epsilon_2 = 4.4389$ MeV. The spectrum shows a sequence of compound resonances, generated by the $\frac{1}{2}^-$, $\frac{1}{2}^+$, and $\frac{5}{2}^+$ bound (single-nucleon) states in $^{13}$C. The situation is very similar in the $p + {}^{12}$C process, with one overall energy shift due to the Coulomb interaction. Because of this shift in energy, some of the compound resonances in the $n + {}^{12}$C system become quasicompound ones in the $p + {}^{12}$C case.

We will show that when deformation (which for the nucleon-$^{12}$C system we consider is of quadrupole type and so linked to a parameter $\beta_2$) tends to zero, the compound and quasicompound states tend to pure states. For compound resonances, their widths tend to zero and their centroid energies tend to those of single-particle bound states plus the core excitations $\epsilon_i$. For quasicompound resonances, the widths tend to the natural widths of the single-particle resonance upon which they are formed, whereas their centroid energies tend to those of the single-particle resonance plus the core excitations $\epsilon_i$. It is interesting then to analyze the behavior of the phenomenology contained in the model as $\beta_2$ varies continuously from the deemed physical value to zero. There is a double purpose to this, namely, to check the rules outlined here in a significant physical case and to describe the spectroscopy of $^{13}$C and $^{13}$N in terms of the scheme specified.

In Sec. II, we discuss the results on the $n + {}^{12}$C system, some of which were reported previously [1]. But now we analyze the origin of each state by studying results in the zero-deformation limit. In Sec. III, the same analysis is extended to a study of the $p + {}^{12}$C system, where the Coulomb shift transforms some of the compound resonances into quasicompound ones. All calculations of this system have been carried out assuming charge symmetry. The potentials that gave the results discussed in Sec. II (and previously [1]) have been used without change. We present conclusions we have drawn from these studies in Sec. IV.

## II. THE $^{13}$C SYSTEM

Calculations of the $n + {}^{12}$C system have been carried out with the parameters defining the initiating nucleon-nucleus interaction matrix of potentials being those used previously [1]. They are presented again in Table I for easy reference.

Couplings of the input channel with the ground state ($\epsilon_1 = 0$) and with the $2^+$ ($\epsilon_2 = 4.4389$ MeV) and $0_2^+$ ($\epsilon_3 = 7.6542$ MeV) excited states of the $^{12}$C target have been considered. Moreover, the Pauli principle has been taken into account throughout using the OPP procedure [1,3]. However, note that the OPP treatment [1] we use is an approximation. We have used a large but finite strength in place of the infinite value that the OPP theory presumes. One must thus expect some small spuriosity, which may affect our calculated energies but by about a tenth of an MeV at worst.

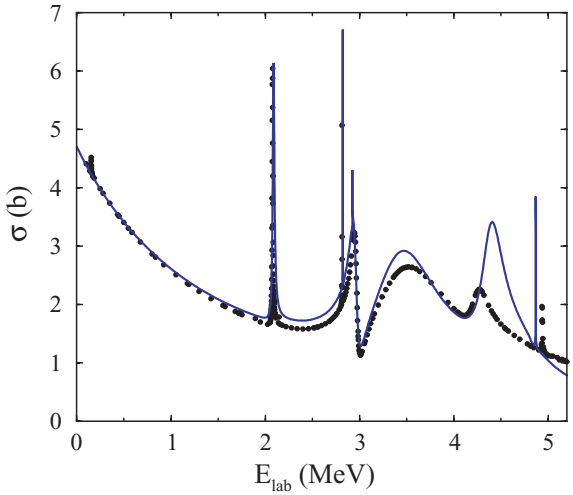


FIG. 1. (Color online) Comparison between data (filled circles) and theoretical (solid curve) calculated elastic scattering cross sections for $n + {}^{12}$C scattering to ∼5 MeV.

In Fig. 1, our calculated $n + {}^{12}$C elastic cross section is compared with data taken from the evaluated nuclear data file (ENDF) formed by Pearlman [6]. Source data and references were obtained using the computer index of neutron data (CINDA) [7]. The energies are in the laboratory frame.

The sequence of resonances evident therein as energy increases have spin-parity assignments $\frac{5}{2}^+$, $\frac{7}{2}^+$, $\frac{1}{2}^-$, $\frac{3}{2}^+$, $\frac{3}{2}^+$, $\frac{5}{2}^+$, and $\frac{9}{2}^+$. Details of those resonances and of bound states are compared with experimental values [8] in Table II. We have found the parameters of the resonances by studying the trajectories of the Sturmian eigenvalues using the algorithm defined in Ref. [1]. This we defined as the resonance identification (RI) process. As already noticed in Ref. [1], this choice is unambiguous in the case of narrow resonances, whereas for wider resonances it represents just one of the possible methods for resonances identification. Note that, in this table, the energies of the states (in MeV) are given in the center-of-mass (c.m.) system. The widths are expressed in keV.

In the first column of Table II we give an identifying index ($i$) to each state that we use throughout the following discussion.

In the spectrum, the $\frac{1}{2}^-$ ($i = 2$) resonance is not seen experimentally. However, from our model calculation it is practically coincident with the first and strong $\frac{3}{2}^+$ resonance ($i = 6$) and is shown in the figure like a narrow spike over the broader $\frac{3}{2}^+$ peak. Possibly that is why it has not been seen in experiments to date. But an isobaric analog to this has been observed in $^{13}$N, and its nature is well explained within the general logic of the spectroscopic structure we believe to be

TABLE II. Subthreshold bound states and low-energy resonances of the $n + {}^{12}$C system.

| entry ($i$) | $J^\pi$ | $E_{\rm exp}$ (MeV) | $\frac{1}{2}\Gamma_{\rm exp}$ (keV) | $E_{\rm th}$ (MeV) | $\frac{1}{2}\Gamma_{\rm th}$ (keV) |
|---|---|---|---|---|---|
| 1 | $\frac{1}{2}^-$ | −4.9463 | — | −4.8881 | — |
| 2 | $\frac{1}{2}^-$ | — | — | 2.6829 | 0.332 |
| 3 | $\frac{1}{2}^+$ | −1.8569 | — | −2.0718 | — |
| 4 | $\frac{1}{2}^+$ | — | — | 4.6629 | 555 |
| 5 | $\frac{3}{2}^-$ | −1.2618 | — | −1.4783 | — |
| 6 | $\frac{3}{2}^+$ | 2.7397 | 35 | 2.7309 | 40.8 |
| 7 | $\frac{3}{2}^+$ | 3.2537 | 500 | 3.2447 | 447 |
| 8 | $\frac{5}{2}^-$ | 0.1 | — | −0.0338 | — |
| 9 | $\frac{5}{2}^+$ | −1.0925 | — | −1.8619 | — |
| 10 | $\frac{5}{2}^+$ | 1.9177 | 3 | 1.9348 | 9.65 |
| 11 | $\frac{5}{2}^+$ | 3.9314 | 55 | 4.0579 | 126 |
| 12 | $\frac{7}{2}^+$ | 2.547 | $\leqslant$2.5 | 2.6220 | $8.74 \times 10^{-4}$ |
| 13 | $\frac{9}{2}^+$ | 4.534 | 2.5 | 4.5091 | 0.745 |

sensible. The very narrow $\frac{5}{2}^-$ resonance ($i = 8$) that lies just above threshold, has a partner in our calculations, but as a bound state just below threshold.

The peak shown in Fig. 1 at an energy of about 4.40 MeV in the laboratory frame (4.06 MeV in the c.m. system) corresponds to our calculated $\frac{5}{2}^+$ ($i = 11$) resonance. In the neighborhood the model also predicts (by using the RI procedure) a $\frac{1}{2}^+$ resonance ($i = 4$) whose centroid energy is $E_{\rm lab} = 5.05$ MeV ($E_{\rm c.m.} = 4.66$ MeV). No corresponding peak is seen in the elastic cross section. In fact, that resonance is missing entirely in Fig. 1. To solve this puzzle we calculated the even-parity components of the cross section separately; that is, the cross section was calculated for the unique $J^\pi$ value of $\frac{1}{2}^+$, then with $\frac{3}{2}^+$, etc. The results shown in Fig. 2 clearly identify the component responsible for each even-parity resonance. The only peak not accounted for in the analysis is that having a spin-parity $\frac{1}{2}^-$. In particular, under the maximum at about 4.4 MeV, there are two overlapping resonances. They are the $\frac{5}{2}^+$ component, which has a sharp maximum in the energy region under consideration, and the $\frac{1}{2}^+$ component, revealed as a very small bump at about the same energy. It is a very broad resonance. The $\frac{1}{2}^+$ component is more easily recognized in the calculated cross section when, as we discuss later, the deformation is decreased.

Thus the cross section is, as could be expected, a dominantly $s$-wave background with strong narrow and broad resonances superimposed. The individual values of energy at which the $s$-wave cross section initially was calculated are represented by the $\times$ symbols in the plot for $J^\pi = \frac{1}{2}^+$. The clustering of $\times$'s (around regions in which sharp resonances in the total cross section occur) reflects the density of mesh points used to find the variation through those regions as precisely as possible. Such a requirement is further evidence of the need in any such study to ensure that all resonance centroids and half widths

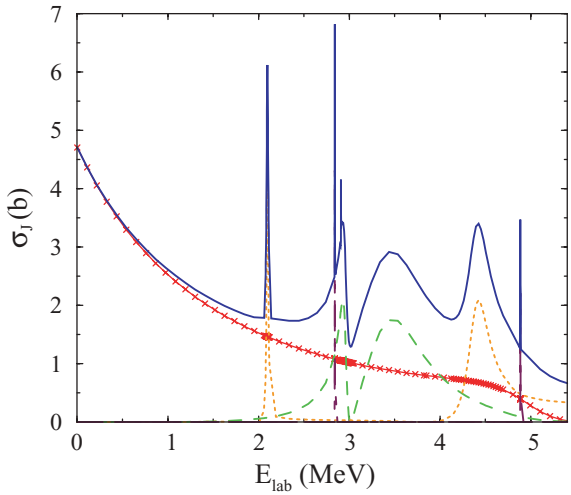


FIG. 2. (Color online) Components in the $n + {}^{12}$C elastic cross section. The theoretical curve (solid curve) is decomposed into its even-parity components. The $\frac{1}{2}^+$ component is shown by the generally smooth curve connecting "$\times$" marks. It constitutes virtually the entire cross section at energies near threshold. The $\frac{3}{2}^+$ and $\frac{5}{2}^+$ components are portrayed by the dashed and dotted curves, respectively. The narrow $\frac{7}{2}^+$ and $\frac{9}{2}^+$ resonances at (lab) energies of 2.84 and 4.88 MeV, respectively, are portrayed by long dashed curves.

are defined in the process and that energy steps in that region are selected appropriately; otherwise with too large an energy step they will be missed. The RI procedure [1] ensures all resonances will be found in the overall energy regime to be studied. Also built into the code implementing this procedure is an automatic increase in numbers of energy points. The span of those points depends on the half width of the resonance, as defined by the RI procedure.

We conclude therefore that the 4.4-MeV peak in the measured cross section is mainly a $\frac{5}{2}^+$ resonance. The $\frac{1}{2}^+$ resonance foreseen by the model calculations is weak and completely masked by it. The effect may be understood better by studying the (c.m.) energy variation of the $\frac{1}{2}^+$ (total) scattering phase shift. That variation is displayed in Fig. 3.

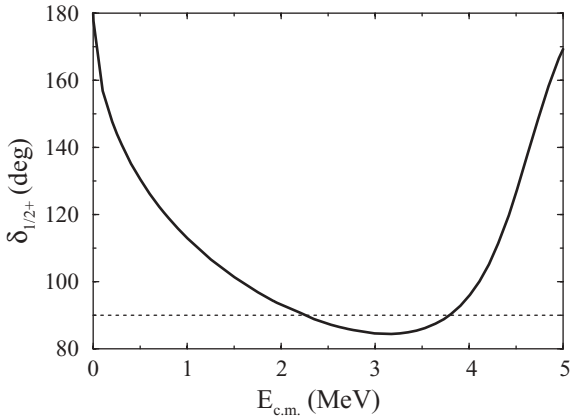


FIG. 3. Energy variation of the calculated $\frac{1}{2}^+$ scattering phase shift.

This phase shift does not exhibit a regular increment between 0° and 180° (as do the other resonant phase shifts), but starts from 180° (because of Levinson's theorem) at zero energy, crosses twice the value of 90° between 2 and 4 MeV, and then increases again toward a value of 180°. That variation between 4 and 5 MeV relates to a broad and not very pronounced peak in the partial cross section, as shown in Fig. 2. Hence we assign our $\frac{5}{2}^+$ ($i = 11$) level with the well-defined experimental resonance at $E_{\text{c.m.}} = 3.9314$ MeV rather than as the $\frac{1}{2}^+$ state heretofore assumed in the literature [8].

The agreement between theory and experiment shown in Fig. 1 and in Table II is very good. Energies of both bound and resonance states, and the widths of those resonances, are quite well matched, particularly so when one recalls that the target structure has been taken within a simple rotational model scheme. A measure of the goodness of fit is the mean-square error in the table entries. That measure formed using eleven of the states is

$$\mu = \frac{1}{N}\sqrt{\sum (E_{\text{th}} - E_{\text{exp}})^2} = 0.0776 \text{ MeV}. \qquad (1)$$

Entries $i = 2$ and $i = 4$ have been omitted because the first has not been detected experimentally and for the second, we propose a different assignment of quantum numbers.

Our procedure enables us to interpret the structure of the spectra by following the general discussion that has been given [9] about the properties of compound resonances. Consider first the even-parity states. These can be specified in the chosen representation in terms of pure states that are identified by the set of quantum numbers $\{J^\pi, I, j, \ell\}$. Although the relevant details concerning these sets of quantum numbers have been extensively discussed before [1], it is useful to note here that the single-particle quantum numbers ($l$) and ($j$) can be related to a state of the single nucleon in the mass-13 systems. Then, in the energy range we study, and considering only the effect of the most important couplings (i.e., with the ground and $2^+$ states of $^{12}$C), we list all possible configurations in Table III. The second excited $0_2^+$ state will enter the discussion later in relation to a particular ($\frac{1}{2}^-$) excited state in the mass-13 spectra.

Assuming a shell model single-nucleon spectrum for an additional nucleon coupling to states in $^{12}$C we expect at most three even-parity bound states to be important, namely, those relating to lodgment of that nucleon within the $1s$-$0d$ shell. However, as reported [1], shell model studies suggest that the low excitation mass-13 states dominantly are identifiable with either $0d_{\frac{5}{2}}$ or $1s_{\frac{1}{2}}$ orbit couplings to the ground and $2^+$ states in $^{12}$C. As such, the coupling to the ground state (in $^{12}$C) will provide two states in the compound nucleus with spin-parity values of $\frac{1}{2}^+$ and $\frac{5}{2}^+$. Therefore we expect one doublet and one quintuplet of even-parity states when the coupling is made with the $2^+$ state.

Using this scheme, the bound state $\frac{1}{2}^+$ ($i = 3$ of Table II) in $^{13}$C should be dominantly described as a $1s_{1/2}$ neutron bound to the $^{12}$C ($0^+$) ground state core and identified with the $N = 1$ entry in the table of pure states: This implies a bound state of energy $E \simeq -2$ MeV. Likewise there should be a $\frac{5}{2}^+$ state ($i = 9$ of Table II), which can be identified with the $N = 9$ entry in Table III. Then, when a neutron impinging with energy $\epsilon_2 + E$ loses $\epsilon_2$ to excitation and is bound to the $^{12}$C$^*(2^+)$ core, there should arise a very narrow resonance: a bound state in the continuum for zero coupling. As the coupling increases, this resonance splits, forming a doublet for which the quantum numbers will be $J^\pi = \frac{3}{2}^+$ and $\frac{5}{2}^+$. The first of these we identify with the state $N = 5$ (responsible for the resonant behavior), coupled with an elastic background arising from the effect of the $N = 4$ entry. The second part of the doublet we link to the state $N = 10$ and expect that it is attached to a background state for which $N = 9$. As the deformation ($|\beta_2|$) increases, both the splitting of the doublet and the resonance widths increase. Also, all of the $J$ components contribute since entries $N = 4$, 5, 6, 7, and 8 are involved for $J = \frac{3}{2}$ and those of $N = 9$, 10, 11, 12, 13, and 14 are involved for $J = \frac{5}{2}$. Hence the bound state $\frac{1}{2}^+$ is expected to generate a doublet of compound resonances, and by the same mechanism, the bound state $\frac{5}{2}^+$ when coupled to the $2^+$ state should generate a quintuplet with spin-parities $J\pi = \frac{1}{2}^+, \frac{3}{2}^+, \frac{5}{2}^+, \frac{7}{2}^+$, and $\frac{9}{2}^+$.

TABLE III. Quantum numbers of allowed even-parity basis states ($J^\pi \leqslant \frac{9}{2}^+$).

| $N$ | $J^\pi$ | $I$ | $j$ | $l$ | $N$ | $J^\pi$ | $I$ | $j$ | $l$ |
|---|---|---|---|---|---|---|---|---|---|
| 1 | $\frac{1}{2}^+$ | 0 | $\frac{1}{2}$ | 0 | 14 | $\frac{5}{2}^+$ | 2 | $\frac{9}{2}$ | 4 |
| 2 | $\frac{1}{2}^+$ | 2 | $\frac{3}{2}$ | 2 | 15 | $\frac{7}{2}^+$ | 0 | $\frac{7}{2}$ | 4 |
| 3 | $\frac{1}{2}^+$ | 2 | $\frac{5}{2}$ | 2 | 16 | $\frac{7}{2}^+$ | 2 | $\frac{3}{2}$ | 2 |
| 4 | $\frac{3}{2}^+$ | 0 | $\frac{3}{2}$ | 2 | 17 | $\frac{7}{2}^+$ | 2 | $\frac{5}{2}$ | 2 |
| 5 | $\frac{3}{2}^+$ | 2 | $\frac{1}{2}$ | 0 | 18 | $\frac{7}{2}^+$ | 2 | $\frac{7}{2}$ | 4 |
| 6 | $\frac{3}{2}^+$ | 2 | $\frac{3}{2}$ | 2 | 19 | $\frac{7}{2}^+$ | 2 | $\frac{9}{2}$ | 4 |
| 7 | $\frac{3}{2}^+$ | 2 | $\frac{5}{2}$ | 2 | 20 | $\frac{7}{2}^+$ | 2 | $\frac{11}{2}$ | 6 |
| 8 | $\frac{3}{2}^+$ | 2 | $\frac{7}{2}$ | 4 | 21 | $\frac{9}{2}^+$ | 0 | $\frac{9}{2}$ | 4 |
| 9 | $\frac{5}{2}^+$ | 0 | $\frac{5}{2}$ | 2 | 22 | $\frac{9}{2}^+$ | 2 | $\frac{5}{2}$ | 2 |
| 10 | $\frac{5}{2}^+$ | 2 | $\frac{1}{2}$ | 0 | 23 | $\frac{9}{2}^+$ | 2 | $\frac{7}{2}$ | 4 |
| 11 | $\frac{5}{2}^+$ | 2 | $\frac{3}{2}$ | 2 | 24 | $\frac{9}{2}^+$ | 2 | $\frac{9}{2}$ | 4 |
| 12 | $\frac{5}{2}^+$ | 2 | $\frac{5}{2}$ | 2 | 25 | $\frac{9}{2}^+$ | 2 | $\frac{11}{2}$ | 6 |
| 13 | $\frac{5}{2}^+$ | 2 | $\frac{7}{2}$ | 4 | 26 | $\frac{9}{2}^+$ | 2 | $\frac{13}{2}$ | 6 |

To verify this scheme, we have made calculations starting with the physical situation of having $\beta_2 = -0.52$, and then we form cross sections from calculations in which the coupling is gradually reduced. By that means it is possible to track each state/resonance continuously and so identify the underlying base nature of each state. It is assumed that each resonance conserves its identity in the adiabatic transition from the physical to the unperturbed limit. We portray the results in Fig 4, which shows the general trend that the background cross-section values near threshold increase in size as $|\beta_2|$ decreases. This trend is consistent with the strong subthreshold $s$-wave $\frac{1}{2}^+$ state moving closer to threshold as $|\beta_2|$ decreases. Then what was just a subthreshold state, the $\frac{5}{2}^-$ in the physical case calculation, moves into the positive energy regime with decrease in $|\beta_2|$. That state has an extremely

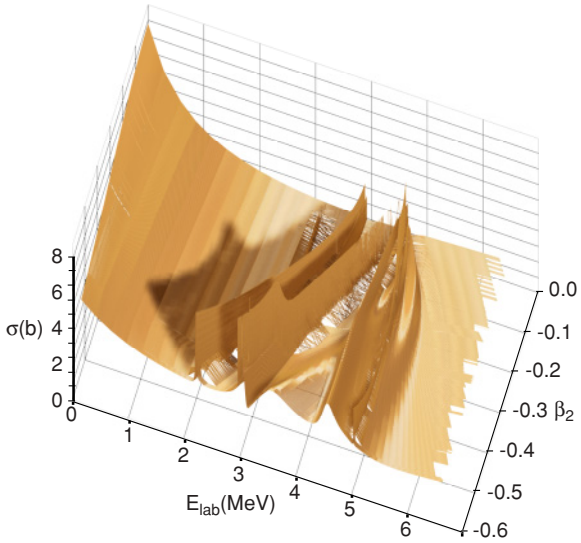


FIG. 4. (Color online) Total elastic cross sections for $n + {}^{12}$C scattering as functions of neutron energy, showing the effects of reducing the value of $\beta_2$. Details are described in the text.

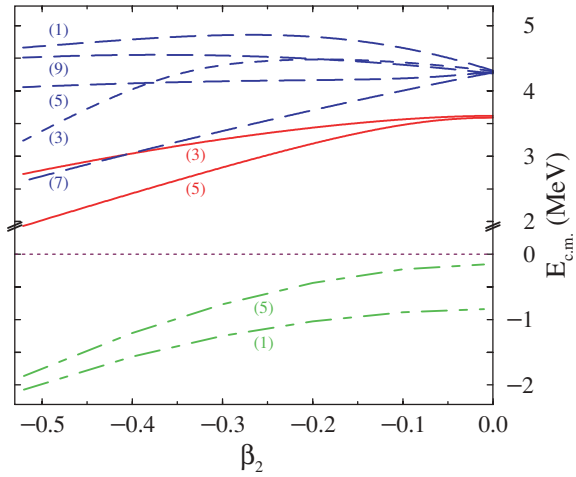


FIG. 5. (Color online) Variation of energies of the $\frac{1}{2}^+$ bound and doublet states and of the $\frac{5}{2}^+$ bound and quintuplet states with deformation. The numbers in brackets attached to each curve are the specific values of $2J$.

small width ($\leqslant 10^{-11}$ MeV) so that although its existence is known, its strength has not been ascertained. The actual resonances also have unique trends with decreasing $|\beta_2|$. With their identification (the entry "$i$" specified in Table II), the narrow $\frac{5}{2}^+$ ($i = 10$) and the first $\frac{3}{2}^+$ ($i = 6$) states track smoothly with decreasing width till they have essentially the same centroid energy and vanishing width; these features will be discussed subsequently. The very narrow $\frac{7}{2}^+$ ($i = 12$) resonance initially sits upon the $\frac{3}{2}^+$ resonance shape and its centroid increases in value with decreasing $|\beta_2|$. It remains a feature upon the $\frac{3}{2}^+$ shape until $|\beta_2| \preceq 0.35$, after which that $\frac{7}{2}^+$ centroid moves up in energy to be one of the quintuplet of sharp resonances at ∼4.3 MeV. The other four members of the quintuplet are the very broad second $\frac{3}{2}^+$ ($i = 7$), the reasonably broad strong $\frac{5}{2}^+$ ($i = 11$), the sharp $\frac{9}{2}$ ($i = 13$), and the reasonably broad but weak $\frac{1}{2}^+$ (∼4.6 MeV) resonances. The last is not readily seen until, with decreasing $|\beta_2|$, the width of the nearby $\frac{5}{2}^+$ resonance decreases sufficiently. In the figure, this $\frac{1}{2}^+$ resonance is seen as the highest energy track that curves back in energy to meet the rest of the quintuplet when $\beta_2 = 0$. The $\frac{9}{2}^+$ resonance sits initially on the tail of the $\frac{5}{2}^+$ resonance, appearing to gradually decrease in size (because the $\frac{5}{2}^+$ resonance is contracting as $|\beta_2|$ decreases) before some enhancement at small values of $|\beta_2|$ resulting from the proximity of all members of the quintuplet. The centroids of the two broad resonances (the $\frac{3}{2}^+$ and the $\frac{5}{2}^+$) of this quintuplet cross as $|\beta_2|$ decreases and while each width gradually decreases, they combine to form quite distinctively changing cross sections until, as $\beta_2 \to 0$, they become very narrow and tend to the same centroid energy. Of course, when $\beta_2$ is exactly zero, since the widths are vanishingly small, a calculated cross section loses almost all trace of individual compound resonances. Nevertheless, by means of the RI procedure, the resonance centroid energies may still be (and were) found.

In Fig. 5 we show our results of the calculations of the centroids of the positive-parity resonances and subthreshold bound states.

Consider first the states built upon a $\frac{5}{2}^+$ single-particle state. They are the quintuplet of resonances having spin-parities $J^\pi = \frac{1}{2}^+, \frac{3}{2}^+, \frac{5}{2}^+, \frac{7}{2}^+$, and $\frac{9}{2}^+$ plus the subthreshold (bound) state in $^{13}$C. Their energy values when $\beta_2 = 0$ (i.e., ∼−0.15 and 4.28) equate to the target excitation $4.28 - (-0.15) = 4.43 \simeq \epsilon_2$, and so we conclude that the quintuplet indeed is a set of compound resonances due to coupling of a $\frac{5}{2}^+$ neutron with the $2^+$ excited state of $^{12}$C and that the $0d_{5/2}$ nucleon binding to the ground state of $^{12}$C is ∼−0.15 MeV. In a similar way, the $\frac{1}{2}^+$ bound state ($i = 3$) has a binding to the ground state of $^{12}$C of ∼−0.83 MeV and the doublet of resonances ($i = 6$ and 10) relate in energy to identify their origins as the $\frac{3}{2}^+, \frac{5}{2}^+$ doublet of states generated by that $\frac{1}{2}^+$ neutron being coupled to the $2^+$ excited state in $^{12}$C. In the zero-deformation limit, the energies of the bound and collapsed doublet states are ∼−0.83 and 3.60 MeV, respectively, thereby differing by the $4.43 \simeq \epsilon_2$ value.

This leads to a complete understanding of the spectroscopy of the even-parity states in $^{13}$C as they are revealed by low-energy $n + {}^{12}$C scattering. Note that the two $\frac{3}{2}^+$ states ($i = 6$ and 7) that come from analysis solely of the scattering data basically are indistinguishable because only $J^\pi$ is conserved. Nevertheless, we expect that $i = 6$ is part of the doublet and $i = 7$ is part of the quintuplet because of the continuity in the limit $\beta_2 \to 0$. Of course, similar information should be obtained by large-space structure model analyses of the wave functions in the two cases. Work is in progress to do just that.

We note that the $\beta_2 = 0$ limit values of energies of the even-parity states discussed tend only approximately to the same values. There are small but significant shifts. That effect is due to the residual operator character of the interaction

TABLE IV. Properties of the even-parity quintuplet of resonances in the limit $\beta_2 = 0$.

| $n$ | $J^\pi$ | $E_{\rm th}$ (MeV) | $K(\ell, j, j, J)$ | $\Delta E_{\rm th}$ (MeV) | $\Delta K$ | $\lvert\frac{\Delta K}{\Delta E_{\rm th}}\rvert$ (MeV$^{-1}$) |
|---|---|---|---|---|---|---|
| 4 | $\frac{1}{2}^+$ | 4.3094 | −14 | — | — | — |
| 7 | $\frac{3}{2}^+$ | 4.3039 | −11 | −0.0055 | 3 | 545 |
| 11 | $\frac{5}{2}^+$ | 4.2948 | −6 | −0.0091 | 5 | 549 |
| 12 | $\frac{7}{2}^+$ | 4.2820 | 1 | −0.0128 | 7 | 546 |
| 13 | $\frac{9}{2}^+$ | 4.2656 | 10 | −0.0164 | 9 | 548 |

potentials. Although the coupling between the channels caused by deformation was removed, there remain some linkages arising from the diagonal potentials being

$$V_c(r) \equiv V_{\rm cc}(r) = [V_0 + \ell(\ell+1)V_{\ell\ell}]\, f_0(r) - \frac{1}{ar} W_{\rm ls} A(r)[\mathbf{l}\cdot\mathbf{s}]_{\rm cc} + V_{\rm ss} f_0(r)[\mathbf{s}\cdot\mathbf{I}]_{\rm cc}. \quad (2)$$

This is the reduced form of Eq. (B.5) of Ref [1], in the limit $\beta_2 \to 0$, where it is meant that the channel index $c$ denotes the set of quantum numbers $\{J^\pi, I, j, \ell\}$. Clearly this discussion fails to hold exactly in the presence of a spin-spin interaction. How much so is illustrated by the entries in Table IV.

In this table we have selected the states of the even-parity quintuplet, and we show in column 3 the calculated values of the unperturbed energies. They reveal the small defects of convergence caused by the spin-spin (target) specific potential term. It is easy to recognize that the members of the even-parity quintuplet (in the unperturbed conditions) are pure states of the type $N = 3$, 7, 12, 17, and 22, as given in Table III with quantum numbers $c \equiv \{\frac{1}{2}^+, 2, \frac{5}{2}, 2\}$, $\{\frac{3}{2}^+, 2, \frac{5}{2}, 2\}$, $\{\frac{5}{2}^+, 2, \frac{5}{2}, 2\}$, $\{\frac{7}{2}^+, 2, \frac{5}{2}, 2\}$, and $\{\frac{9}{2}^+, 2, \frac{5}{2}, 2\}$, respectively. These states differ (only) in the total angular momentum $J$ and therefore are discriminated (only) by the spin-spin part of the potential.

In particular, from Eqs. (B8), (B9), and (B10) of Ref. [1], it may be seen that the spin-spin potential eigenvalues depend on the quantum number $J$ through functions $K(\ell, j, j', J)$. Those numbers are listed in column 4 of Table IV. To verify the proportionality of the values of $E_{\rm th}$ and $K$, we give the differences $\Delta E_{\rm th}$ between adjacent states in the list [i.e., $E_{\rm th}(i = 7) - E_{\rm th}(i = 4)$, etc.] in column 5. Then, in column 6, the associated differences $\Delta K$ [namely, $K(i = 7) - K(i = 4)$, etc.] are given; in column 7 we present the ratios $\Delta K/\Delta E_{\rm th}$. The value reported in the last column is constant within 0.4%, most readily confirming the assumption that the degeneracy of the multiplet in the unperturbed limit is broken only by the spin-spin interaction. Therefore we have repeated calculations with $\beta_2 = 0$ but additionally with the spin-spin potential set to zero. All other parameters remain the same as those values given in Table I. The energies of the states then found are presented in Table V. Therein also, in the rightmost column, we give the gap energies $\Delta E_i$, which are the differences between the resonance energies of the listed value and of the bound-state energy of the particle coupled to the $^{12}$C ground state. Therein the states for $i = 1$, 3, and 9 are taken as coupling a $0p_{1/2}$, $1s_{1/2}$, and a $0d_{5/2}$ neutron, respectively, to the ground state of $^{12}$C. Then all of the remaining differences shown in the last column (except for the $i = 2$ case) are exactly the assumed excitation energy of the $2^+$ state in $^{12}$C ($\epsilon_2$). As already observed, our assumption is that the even-parity quintuplet, $i = 4$, 7, 11, 12, and 13, derives from the bound state giving $i = 9$ (and therefore the definitions of the gap energies are $\Delta E_4 = E_4 - E_9$, $\Delta E_7 = E_7 - E_9$, etc), whereas the even-parity doublet, $i = 6$ and 10, derives from the bound state that leads to $i = 3$ (and therefore $\Delta E_6 = E_6 - E_3$, $\Delta E_{10} = E_{10} - E_3$). The $i = 2$ entry results from the coupling of the $0p_{1/2}$ (that gave $i = 1$) to the third state we chose to include in the target spectrum used in MCAS. This is the only effect of the excitation of the $0_2^+$ excited state in $^{12}$C, at least for the energy range we have considered. To explore more effects of the $0_2^+$ state, higher energy results need to be analyzed. But then one would also need to consider effects of other states such as the strong collective $3^-$ (9.63 MeV).

As far as the other odd-parity states are concerned, the values listed in Table V strongly suggest that the states $i = 5$ and $i = 8$ (the latter of which is reproduced as a near-threshold bound state in our calculations) are the result of coupling a $0p_{1/2}$ neutron (as identified in the $i = 1$ level) with the $2^+$ excited state in $^{12}$C. All these conclusions about the odd states

TABLE V. Subthreshold bound states and resonances in $n + {}^{12}$C when $\beta_2 = 0$ and $V_{ss} = 0$.

| $i$ | $J^\pi$ | $E_{\rm th}$ (MeV) | $\Delta E_i$ (MeV) |
|---|---|---|---|
| 1 | $\frac{1}{2}^-$ | −4.7017 | 0 |
| 2 | $\frac{1}{2}^-$ | 2.9525 | 7.6542 |
| 3 | $\frac{1}{2}^+$ | −0.8376 | 0 |
| 4 | $\frac{1}{2}^+$ | 4.2839 | 4.4389 |
| 5 | $\frac{3}{2}^-$ | −0.2627 | 4.4390 |
| 6 | $\frac{3}{2}^+$ | 3.6013 | 4.4389 |
| 7 | $\frac{3}{2}^+$ | 4.2839 | 4.4389 |
| 8 | $\frac{5}{2}^-$ | −0.2627 | 4.4390 |
| 9 | $\frac{5}{2}^+$ | −0.1550 | 0 |
| 10 | $\frac{5}{2}^+$ | 3.6013 | 4.4389 |
| 11 | $\frac{5}{2}^+$ | 4.2839 | 4.4389 |
| 12 | $\frac{7}{2}^+$ | 4.2839 | 4.4389 |
| 13 | $\frac{9}{2}^+$ | 4.2839 | 4.4389 |

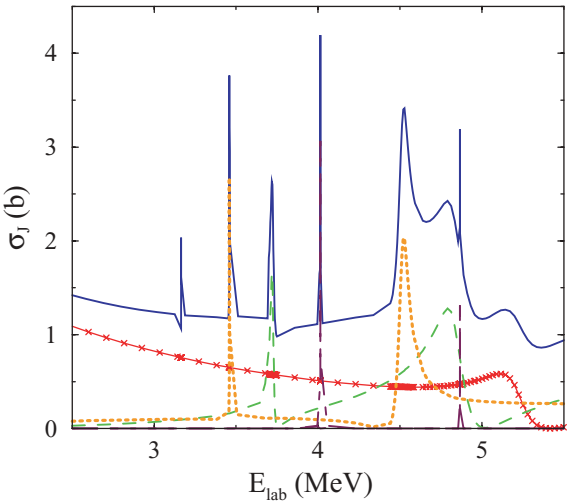


FIG. 6. (Color online) Even-parity-component contributions to the elastic $n + {}^{12}$C cross sections in the case of small deformation ($\beta_2 = -0.2$). In this case the narrow $\frac{7}{2}^+$ and $\frac{9}{2}^+$ resonances lie at (lab) energies of 4.0 and 4.8 MeV, respectively.

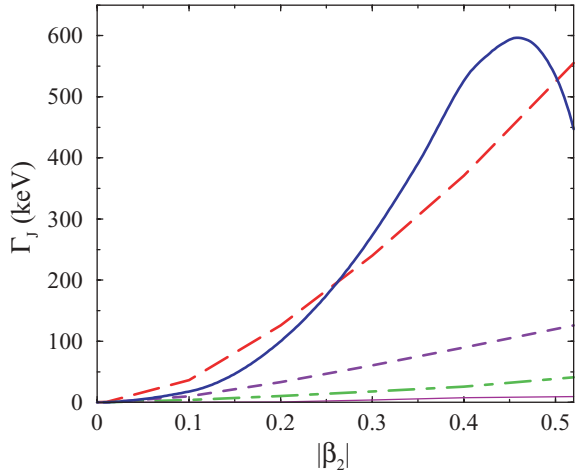


FIG. 7. (Color online) Deformation dependence of widths $\Gamma_{\rm th}(J^\pi)$ (in keV) for some of the (broader) compound resonances. Those from cases with $i = 4$, 6, 7, 10, and 11 are portrayed by the long dashed, dot-dashed, solid, thin solid, and dashed curves, respectively.

may be drawn only after dropping the spin-spin term, because the spin-spin interaction is stronger for the odd states (see Table I) and masks completely the effect of the convergence in the unperturbed limit.

Finally, with the $n + {}^{12}$C system, in Fig. 6 we show the even-parity components of the cross sections but now when a small finite deformation $\beta_2 = -0.2$ has been used. In this case only cross sections in the energy range 2.4–5.5 MeV are displayed, which suffice to show the three groupings of interest. The resonances seen in the total elastic cross section for this (small) deformation in sequence as energy increases have spin parities $\frac{1}{2}^-$, $\frac{5}{2}^+$, $\frac{3}{2}^+$, $\frac{7}{2}^+$, $\frac{5}{2}^+$, $\frac{3}{2}^+$, $\frac{9}{2}^+$, and $\frac{1}{2}^+$. The total cross section is depicted by the solid curve. The notation for the separate component even-parity cross sections is as given for Fig. 2.

By comparison with results shown previously, we note the following:

(1) The resonances can be assembled into three groups: an odd-parity singlet, an even-parity doublet, and an even-parity quintuplet.

(2) The $\frac{1}{2}^+$ resonance ($i = 4$), though registered through the RI procedure but not evident as a peak in the cross section in Fig. 1, now is seen as a little bump in the cross section above 5 MeV. Of the even-parity components, the $\frac{1}{2}^+$ one, which dominates the lowest energy values, clearly identifies that highest energy resonance in this figure as having that spin parity.

(3) The widths are smaller than those found in Fig. 1, as was also very evident in the three-dimensional diagram (Fig. 4). They all tend to zero as $|\beta_2|$ is gradually taken to zero, thereby confirming the nature of all of the compound resonances analyzed. To illustrate that variation in the widths $\Gamma$, a select set of those for some of the larger resonances are plotted versus the deformation $\beta_2$ in Fig. 7. As foreseen by theory [9], the widths tend to zero as $|\beta_2|^2$. Note that in one case ($i = 7$), $\Gamma_{\rm th}(J^\pi = \frac{3}{2}^+)$ initially increases as $|\beta_2|$ decreases. This is due to the coupling being quite strong so that the physical regime is far from the unperturbed limit.

(4) We have verified that with the small value for deformation, the $i = 8$, $\frac{5}{2}^-$ state is a resonance, a bound state in the continuum. For the physical value of $\beta_2 = -0.52$, it is an actual subthreshold bound state.

## III. THE $^{13}$N SYSTEM

In analyzing the $^{13}$N system we have assumed charge symmetry, and so we use the parameter values given in Table I for the $n + {}^{12}$C system to evaluate $p + {}^{12}$C scattering and to assess properties of the subthreshold compound nucleus $^{13}$N. Only a Coulomb interaction has been added. For simplicity we have chosen the Coulomb potential to be that of a uniformly charged sphere so that we have only one new parameter, the Coulomb radius $R_c$. The best agreement with the experimental data has been obtained with the value $R_c = 2.4$ fm.

The results, centroid energies and widths, are listed in Table VI and are compared therein with experimental data [8].

The comparison is quite good with the mean-square error $\mu$, as specified by Eq. (1), relative to 13 states of Table VI being 0.2563 MeV. The entry in row 11 has been excluded from the sum since there is no experimental counterpart to that state. The average of the differences between pairs of states in $^{13}$N and $^{13}$C with reference to the experimental and theoretical spectra, respectively, are the following:

$$\begin{aligned} \langle E_{\rm exp}(^{13}{\rm N}) - E_{\rm exp}(^{13}{\rm C})\rangle &= 3.01\,{\rm MeV}; \\ \langle E_{\rm th}(^{13}{\rm N}) - E_{\rm th}(^{13}{\rm C})\rangle &= 2.54\,{\rm MeV}. \end{aligned} \tag{3}$$

Thus, through coupling with the $2^+$ level, the bound state underlying the $i = 1$ entry generates the compound odd-parity doublet $i = 5$ and 8 in the tabulation, and that underlying the resonance for $i = 3$ generates the quasicompound even-parity

TABLE VI. Comparison between experiment and theory for the $p + {}^{12}$C system.

| $i$ | $J^\pi$ | $E_{\rm exp}$ (MeV) | $\frac{1}{2}\Gamma_{\rm exp}$ (keV) | $E_{\rm th}$ (MeV) | $\frac{1}{2}\Gamma_{\rm th}$ (keV) |
|---|---|---|---|---|---|
| 1 | $\frac{1}{2}^-$ | −1.9435 | — | −1.9104 | — |
| 2 | $\frac{1}{2}^-$ | 6.9745 | 115 | 5.6391 | 17.8 |
| 3 | $\frac{1}{2}^+$ | 0.4214 | 15.8 | −0.0158 | — |
| 4 | $\frac{1}{2}^+$ | 8.3065 | 140 | 6.9911 | 995 |
| 5 | $\frac{3}{2}^-$ | 1.5675 | 31 | 1.5793 | 11.1 |
| 6 | $\frac{3}{2}^+$ | 4.9425 | 57.5 | 4.7280 | 44.5 |
| 7 | $\frac{3}{2}^+$ | 5.9565 | 750 | 5.8942 | 653 |
| 8 | $\frac{5}{2}^-$ | 5.4325 | 37.5 | 2.9281 | $3.38 \times 10^{-3}$ |
| 9 | $\frac{5}{2}^+$ | 1.6035 | 23.5 | 0.6379 | 0.899 |
| 10 | $\frac{5}{2}^+$ | 4.4205 | 5.5 | 4.1794 | 8.86 |
| 11 | $\frac{5}{2}^+$ | — | — | 6.5281 | 726 |
| 12 | $\frac{7}{2}^+$ | 5.2115 | 4.5 | 5.1234 | 1.50 |
| 13 | $\frac{9}{2}^+$ | 7.0565 | 140 | 6.8341 | 153 |
| 14 | $\frac{5}{2}^+$ | 9.5865 | 215 | 9.7895 | 910 |

doublet $i = 6$ and 10. Likewise, the resonance $i = 9$ links to the quasicompound even-parity quintuplet formed by the $i = 4$, 7, 11, 12, and 13 entries in Table VI. Finally, the $i = 1$ bound state when coupled with the second $0^+$ level gives rise to the single compound resonance for $i = 2$.

For confirmation, in Table VII we give the results of calculations of the $p + {}^{12}$C system in the unperturbed limit ($\beta_2 = 0$) with the spin-spin term set to zero.

The fourth column shows the differences that are consistent with the couplings we suggest. All the members of each multiplet tend to the same limit, and the difference between this limit and the relative *generator* single-particle state

TABLE VII. Subthreshold bound states and resonances in $p + {}^{12}$C when $\beta_2 = 0$ and $V_{\rm ss} = 0$.

| $i$ | $J^\pi$ | $E_{\rm th}$ (MeV) | $\Delta E_n$ (MeV) | $\frac{1}{2}\Gamma_{\rm th}$ (keV) |
|---|---|---|---|---|
| 1 | $\frac{1}{2}^-$ | −1.6785 | 0 | — |
| 2 | $\frac{1}{2}^-$ | 5.9757 | 7.6542 | 0 |
| 3 | $\frac{1}{2}^+$ | 1.0217 | 0 | 468 |
| 4 | $\frac{1}{2}^+$ | 6.6841 | 4.4389 | 115 |
| 5 | $\frac{3}{2}^-$ | 2.7604 | 4.4389 | 0 |
| 6 | $\frac{3}{2}^+$ | 5.4606 | 4.4389 | 467 |
| 7 | $\frac{3}{2}^+$ | 6.6841 | 4.4389 | 115 |
| 8 | $\frac{5}{2}^-$ | 2.7603 | 4.4388 | 0 |
| 9 | $\frac{5}{2}^+$ | 2.2452 | 0 | 115 |
| 10 | $\frac{5}{2}^+$ | 5.4606 | 4.4389 | 466 |
| 11 | $\frac{5}{2}^+$ | 6.6841 | 4.4389 | 115 |
| 12 | $\frac{7}{2}^+$ | 6.6841 | 4.4389 | 115 |
| 13 | $\frac{9}{2}^+$ | 6.6841 | 4.4389 | 115 |
| 14 | $\frac{5}{2}^+$ | 9.8995 | 7.6543 | 115 |

corresponds to the energy of the relevant target excited state involved in the coupling. But there are some differences. For example, the proton calculations predict four $\frac{5}{2}^+$ resonances in the energy range selected. That is one more than found from the neutron calculations in an equivalent energy range. Also, whereas the $\frac{5}{2}^+$ resonances $i = 9$, 10, and 11 are, respectively, the single-particle state, a component of the even-parity doublet, and a component of the even-parity quintuplet as found in the neutron case, the $i = 14$ resonance is new. Our $\beta_2 \to 0$ analysis indicates that this (extra) state originates from the coupling to the excited $0_2^+$ state in $^{12}$C.

An analysis of the widths listed in Table VII is interesting. In the past [9], it was noted that the width of the compound resonance (derived from a purely mathematical example), approaches zero as the coupling approaches zero (because its origin was a bound state), whereas the width of the quasicompound ones tend to the natural width of the resonance from which such originated. It is evident in Table VII that the odd-parity doublet ($i = 5$ and 8) and the odd-parity resonance ($i = 2$) are compound resonances as their widths vanish in the limit of zero deformation. The even-parity quintuplet ($i = 4, 7, 11, 12,$ and 13) and the resonance ($i = 14$) have the width of the common resonance partner ($i = 9$) and so are quasicompound resonances. The width of the quasicompound even-parity doublet ($i = 6$ and 10) is that of the partner resonance for which $i = 3$.

Thus there is a one-to-one correspondence between the states calculated by the model and those experimentally known, with the exception of the $\frac{5}{2}^+$ resonance ($i = 14$). But that resonance, although missing in $n + {}^{12}$C experimental data, has an observed partner in the $p + {}^{12}$C system. Also, although it is clear from the comparisons to be made within Table VI that the calculated energy centroids generally are in good agreement with data and that the widths concur in order of magnitude, there are some exceptions. In particular, the $\frac{5}{2}^-$ ($i = 8$) state is not well reproduced. Also, state $i = 3$ is very close to threshold and, in spite of the small difference between theory and experiment, calculations make it be a subthreshold bound state instead of a resonance.

Of course, we have adopted a strict charge symmetry assumption and have used a very simple form for the Coulomb interaction. It should be possible to find improved $^{13}$N properties from the MCAS approach with but slight changes of these potentials.

### Proton scattering from $^{12}$C: cross section and analyzing power

Since Coulomb scattering amplitudes diverge at zero degree scattering, measurements of proton scattering do not lead to total elastic scattering cross sections. Instead, the usual procedure is to find cross sections at fixed scattering angles and/or differential cross sections at fixed energies. However, as the MCAS approach yields complete scattering ($S$)-matrices, such angular observables are readily predicted.

For energies to 7 MeV, proton elastic scattering from $^{12}$C at fixed (c.m.) scattering angles of 54° and at 90° are shown in

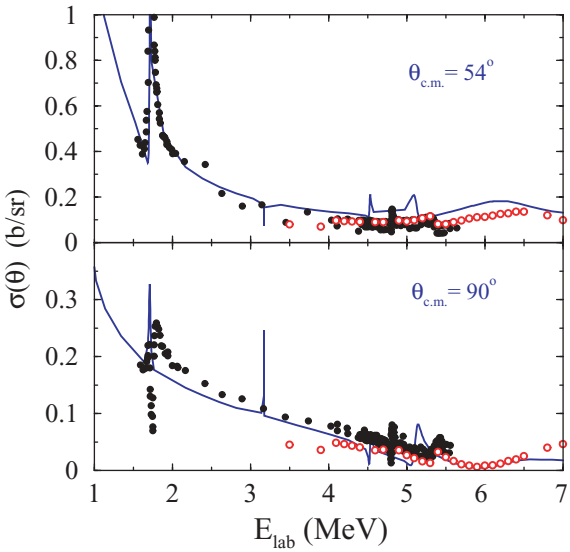


FIG. 8. (Color online) Cross sections from proton elastic scattering from $^{12}$C for two (c.m.) scattering angles, 54° (top panel) and 90° (bottom panel). Details are given in the text.

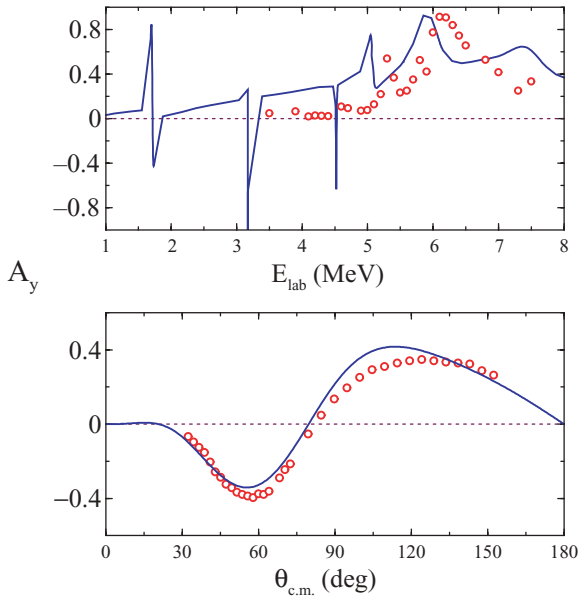


FIG. 9. (Color online) Experimental analyzing powers from proton scattering from $^{12}$C compared with our theoretical calculations. Data and results taken for a range of energies at a fixed scattering angle of 90° are shown in the top panel; angular variations at a fixed energy (of 3.5 MeV) are shown in the bottom panel.

the top and bottom panels of Fig. 8, respectively. Therein our calculated cross sections, shown by the continuous lines, are compared with available data. With energies in the laboratory frame, the data were taken from Ref. [10] (open circles) while those depicted by filled black circles come from Ref. [11].

At 54°, the $\frac{3}{2}^-$ ($i = 5$) resonance in the data is very well reproduced. The other resonances, $\frac{5}{2}^+$ ($i = 10$), $\frac{3}{2}^+$ ($i = 6$), and the broad $\frac{3}{2}^+$ ($i = 7$), also are well reproduced in shape and require but a small shift in energy. That need for a small energy shift is also evident in their centroid values, which are listed in Table VI. The sharp peak shown in the theoretical curves near 3.2 MeV is the $\frac{5}{2}^-$ ($i = 8$) resonance; a state that has been experimentally detected at higher energies. These findings are confirmed by comparison of the calculated results with the data taken at 90° and displayed in the bottom panel.

Usually, analyzing powers $A_y$ from nucleon-nucleus scattering are more sensitive to details of structure than are the differential cross sections. Two results for this observable are presented in Fig. 9. In the top panel of this figure, analyzing powers for proton elastic scattering at 90° (c.m.) and for (lab) energies of 1–8 MeV are depicted. In the bottom panel, angular variation of the analyzing power for a fixed energy of 3.5 MeV is shown.

The experimental data [10] are depicted by open circles and our calculated results are given by the solid curve. The resonances seen in this figure are those that were discussed in relation to Fig. 8. The bottom panel gives an angular variation of analyzing powers for an energy (3.5 MeV) that is well removed from any strong resonance influence. The calculated result then reflects what the model predicts as background effects. The agreement with data is good. Note that no additional parameter variation was done to achieve this agreement.

To investigate deformation effects on differential cross sections, we calculated them again using the values of parameters as listed in Table I but with the deformation parameter $\beta_2 = -0.2$. The results are shown in Fig. 10 for a (c.m.) scattering angle of 90° and (lab) energies ranging between 1 and 6 MeV.

This figure reveals how the single-particle and compound resonances behave with decreased deformation. The $\frac{1}{2}^+$ ($i = 3$) and $\frac{5}{2}^+$ ($i = 9$) single-particle resonances (the first of which was not seen in the preceding figure because it lies too low in energy) maintain their natural width, whereas the $\frac{3}{2}^-$ ($i = 5$) and $\frac{5}{2}^-$ ($i = 8$) compound resonances sharpen. With $\beta_2 = -0.2$, already they are very narrow. The small bump between

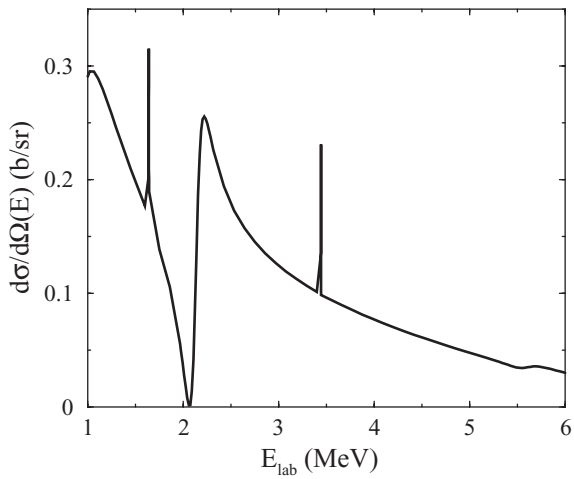


FIG. 10. Energy variation of the theoretical differential cross section for proton scattering from $^{12}$C at a c.m. scattering angle of 90°. The calculation was made using $\beta_2 = -0.2$.

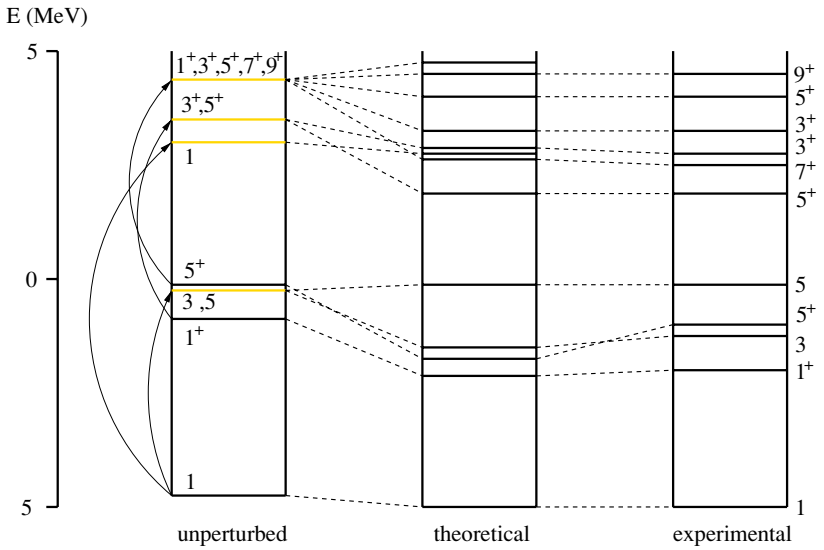


FIG. 11. (Color online) The genesis of the theoretical spectrum for $^{13}$C schematically represented and compared with the experimental spectrum.

5 and 6 MeV corresponds to the $\frac{5}{2}^+$ ($i = 10$) resonance, which maintains its natural width but, being quasicompound, is strongly damped as the unperturbed limit is approached. Thus the behavior of the three kinds of resonances (single-particle, compound, and quasicompound), as the coupling constant is decreased, is just that foreseen previously [9]. Namely, as $\beta$ approaches zero, single-particle resonances conserve their shapes, compound resonances reduce their widths gradually, keeping constant heights, and quasicompound resonances reduce their heights gradually, keeping constant widths.

## IV. CONCLUSIONS

We have analyzed the low-energy spectra of $^{13}$C and $^{13}$N and low-energy data from the elastic scattering of neutrons and of protons on $^{12}$C. Our method of analysis was that of a multichannel algebraic scattering theory with which both the (positive energy) scattering of nucleons from $^{12}$C and (by using negative energies) the subthreshold bound states of the compound nuclei could be predicted. The method, based upon Sturmian expansions of a matrix of interaction potentials, ensures that all subthreshold as well as resonant states within the chosen range of energies are found. Moreover, the approach is adapted so that the Pauli principle is not violated even when a collective model is used to define those interaction potentials. In the cases studied, just such a rotational model was used for that purpose and the $0^+$ (ground), $2^+$ (4.438 MeV), and the $0_2^+$ (7.96 MeV) states in $^{12}$C were taken as active.

The results of our analysis are summarized in Figs. 11 and 12, for the compound nuclei $^{13}$C and $^{13}$N, respectively. Each displays three ladder diagrams; the first two are the results of our calculations (unperturbed resulting when $\beta_2 = 0$) and they are compared with the experimental values (far right).

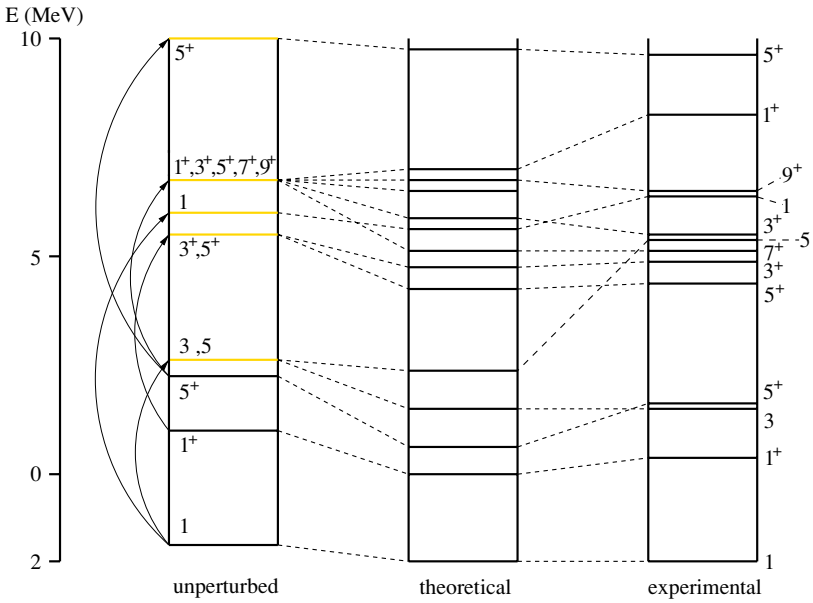


FIG. 12. (Color online) The genesis of the theoretical spectrum for $^{13}$N schematically represented and compared with the experimental spectrum.

Considering Fig. 11 for $^{13}$C first, we note that it supports three (dominantly single-particle) bound states, as is clear from the unperturbed ($\beta_2 = 0$) spectrum depicted on the left of the figure. Those states are highlighted in that spectrum as dark lines. In addition the coupling of the incoming neutron with the excited levels in the target $^{12}$C then gives rise to metastable states whose presumed unperturbed ($\beta_2 = 0$) configurations are represented by lighter lines. They are connected with what we deduced as a partner by the curved lines. The energy gaps between these are $\epsilon_2$ and $\epsilon_3$ as relevant for the two possible cases. These unperturbed resonances are infinitely narrow ($\Gamma_{\rm th} \to 0$) and fully degenerate when one neglects the small effect of the spin-spin interaction in this representation. The finite deformation ($\beta_2 = -0.52$) splits these components to yield the predicted resonances as shown in the middle of the set, which compares very favorably with the experimental spectrum given in the box to the right.

Similar conclusions can be drawn from the spectra of $^{13}$N that is shown in Fig. 12. Also, now, the unperturbed spectrum shows the effects of couplings to the $0_2^+$ core state with the $0p_{\frac{1}{2}}^-$ and $0d_{\frac{5}{2}}^+$ single particle states. There is a similar result from coupling the $1s_{\frac{1}{2}}^+$ to that core state namely a $\frac{1}{2}^+$ state in the unperturbed spectrum at 8.6759 MeV. That level has not been shown in the figure since, with increasing deformation, it is shifted to higher excitation energies out of the range displayed.

Because of the Coulomb energy shift, there is only one subthreshold bound state, and the MCAS approach assuming charge symmetry gives just that and with the correct spin parity. As with the $^{13}$C system, accounting for the Pauli principle is crucial. Otherwise, numerous spurious levels result. An interesting difference, however, is that the Coulomb effect transforms the $\frac{1}{2}^+$ and $\frac{5}{2}^+$ bound states to be single-particle resonances, and owing to coupling with excited core states their products become quasicompound resonances. The different behavior of compound and quasicompound resonances in the limit $\beta_2 \to 0$ confirms statements formulated in a previous paper [9].

We conclude by noting that, with a unique set of potential parameters, the MCAS approach reproduces the data. The results facilitate interpretation of the phenomenology of both the $^{13}$C and $^{13}$N systems in the considered energy range in both a satisfactory and a fairly exhaustive way.

## ACKNOWLEDGMENTS

This research was supported by a grant from the Australian Research Council, by a merit award with the Australian Partners for Advanced Computing, by the Italian MURST-PRIN Project "Fisica Teorica del Nucleo e dei Sistemi a Piú Corpi," and by the Natural Sciences and Engineering Research Council (NSERC), Canada. J. P. S., K. A., and D.v.d.K. acknowledge the hospitality and support of the INFN, Padova, and of the Dipartimento di Fisica, Università di Padova between 1999 and 2004. L. C. and J. P. S. also would like to thank the School of Physics, University of Melbourne, and L.C., G.P., and K.A. acknowledge the hospitality and support of the Department of Physics and Astronomy, University of Manitoba.

[1] K. Amos, L. Canton, G. Pisent, J. P. Svenne, and D. van der Knijff, Nucl. Phys. **A728**, 65 (2003).
[2] L. Canton, G. Cattapan, and G. Pisent, Nucl. Phys. **A487**, 333 (1988).
[3] L. Canton, G. Pisent, J. P. Svenne, D. van der Knijff, K. Amos, and S. Karataglidis, Phys. Rev. Lett. **94**, 122503 (2005).
[4] V. Kukulin and V. Pomerantsev, Ann. Phys. (NY) **111**, 330 (1978).
[5] S. Saito, Prog. Theor. Phys. **41**, 705 (1969).
[6] S. Pearlman, ENDF/HE-VI Mat-625 (1993), BNL-48035.
[7] IAEA-NDS, *Computer Index of Neutron Data* (CINDA), International Atomic Energy Agency, Nuclear Data Services database version of January 4, 2005.
[8] F. Ajzenberg-Selove, Nucl. Phys. **A523**, 1 (1991).
[9] G. Pisent and J. P. Svenne, Phys. Rev. C **51**, 3211 (1995), and references cited therein.
[10] L. Sydow, S. Vohl, S. Lemaitre, P. Nießen, K. R. Nyga, R. Reckenfelderbäumer, G. Rauprich, and H. Paetz gen. Schieck, Nucl. Instrum. Methods **A327**, 441 (1993).
[11] C. W. Reich, G. C. Phillips, and J. L. Russell, Phys. Rev. **104**, 143 (1956).